JOURNAL OF THE AMERICAN COLLEGE OF CARDIOLOGY VOL. 75, NO. 15, 2020

AntimiR-21 Prevents Myocardial Dysfunction in a Pig Model of Ischemia/Reperfusion Injury

Rabea Hinkel, DVM,[a,b,c,d,*] Deepak Ramanujam, PhD,[d,e,*] Veronika Kaczmarek, MD,[a,b] Andrea Howe, DVM,[a,b] Katharina Klett, DVM,[a,b] Christina Beck, MPharm,[d,e] Anne Dueck, PhD,[d,e] Thomas Thum, MD, PhD,[f] Karl-Ludwig Laugwitz, MD,[a,d] Lars Maegdefessel, MD, PhD,[d,g] Christian Weber, MD,[b,d,h] Christian Kupatt, MD,[a,d,†] Stefan Engelhardt, MD, PhD[d,e,†]

ABSTRACT

BACKGROUND miR-21 is a central regulator of cardiac fibrosis, and its inhibition in small-animal models has been shown to be an effective antifibrotic strategy in various organs, including the heart. Effective delivery of therapeutic antisense micro-ribonucleic acid (antimiR) molecules to the myocardium in larger organisms is challenging, though, and remains to be established for models of chronic heart failure.

OBJECTIVES The aims of this study were to test the applicability and therapeutic efficacy of local, catheter-based delivery of antimiR-21 in a pig model of heart failure and determine its effect on the cardiac transcriptomic signature and cellular composition.

METHODS Pigs underwent transient percutaneous occlusion of the left coronary artery and were followed up for 33 days. AntimiR-21 (10 mg) was applied by intracoronary infusion at days 5 and 19 after the injury. Cardiac function was assessed in vivo, followed by histological analyses and deep ribonucleic acid sequencing (RNA-seq) of the myocardium and genetic deconvolution analysis.

RESULTS AntimiR-21 effectively suppressed the remodeling-associated increase of miR-21. At 33 days after ischemia/reperfusion injury, LNA-21-treated hearts exhibited reduced cardiac fibrosis and hypertrophy and improved cardiac function. Deep RNA-seq revealed a significant derepression of the miR-21 targetome in antimiR-21-treated myocardium and a suppression of the inflammatory response and mitogen-activated protein kinase signaling. A genetic deconvolution approach built on deep RNA-seq and single-cell RNA-seq data identified reductions in macrophage and fibroblast numbers as the key cell types affected by antimiR-21 treatment.

CONCLUSIONS This study provides the first evidence for the feasibility and therapeutic efficacy of miR-21 inhibition in a large animal model of heart failure. (J Am Coll Cardiol 2020;75:1788–800) © 2020 The Authors. Published by Elsevier on behalf of the American College of Cardiology Foundation. This is an open access article under the CC BY-NC-ND license (http://creativecommons.org/licenses/by-nc-nd/4.0/).

From the [a]1. Medizinische Klinik und Poliklinik, Klinikum Rechts der Isar, Technische Universität München, Munich, Germany; [b]Institute for Cardiovascular Prevention, Ludwigs-Maximilians-Universität München, Munich, Germany; [c]Deutsches Primatenzentrum GmbH, Leibnitz-Institut für Primatenforschung, Laboratory Animal Science Unit, Göttingen, Germany; [d]DZHK (German Center for Cardiovascular Research), partner site Munich Heart Alliance, Munich, Germany; [e]Institut für Pharmakologie und Toxikologie, Technische Universität München, Munich, Germany; [f]Institute of Molecular and Translational Therapeutic Strategies, Hannover Medical School, Hannover, Germany; [g]Department of Vascular Surgery, Klinikum Rechts der Isar, Technische Universität München, Munich, Germany; and the [h]Department of Biochemistry, Cardiovascular Research Institute Maastricht, Maastricht University, Maastricht, the Netherlands. *Drs. Hinkel and Ramanujam contributed equally to this work. †Drs. Engelhardt and Kupatt share the last authorship. This work was funded by BMBF Munich Biotech cluster m4 (grant BMBF16GW0019 to Drs. Kupatt and Engelhardt) and the German Center for Cardiovascular Research (DZHK). The authors' research is supported by Deutsche Forschungsgemeinschaft (grant TRR267 to Drs. Kupatt, Maegdefessel, Dueck, Laugwitz, Weber, and Engelhardt and grant SFB1123 to Drs. Maegdefessel and Weber) and the European Union (ERA-CVD MacroERA [01KL1706] to Dr. Engelhardt). Dr. Weber is a Van de Laar Professor of atherosclerosis. Drs. Thum and Engelhardt have received royalties from a patent on miR-21 licensed by Uni Würzburg. Dr. Thum is founder and holds shares of Cardior Pharmaceuticals GmbH. All other authors have reported that they have no relationships relevant to the contents of this paper to disclose.

Manuscript received December 12, 2019; revised manuscript received February 5, 2020, accepted February 10, 2020.

Listen to this manuscript's audio summary by Editor-in-Chief Dr. Valentin Fuster on JACC.org.

ISSN 0735-1097 https://doi.org/10.1016/j.jacc.2020.02.041

Although acute survival after myocardial infarction has considerably improved within recent decades (1), postischemic heart failure (HF) remains a very frequent (approximately 50%) consequence and constitutes one of the most common causes of hospitalization and death (1). Although current medical management of HF relies largely on vasodilating agents and inhibitors of neurohumoral activation, the clinical efficacy of these therapeutic principles has been suggested as having reached a level at which further increases in clinical benefit are increasingly difficult to achieve (2). Still, there is an urgent need for new therapeutic strategies targeting alternative mechanisms and molecules involved in HF pathology. One such class of molecules that has emerged as powerful regulators of gene expression are micro-ribonucleic acids (miRs or miRNAs). MiRNAs are tiny (20 to 22 nt long) RNA molecules that bind to antisense complementary regions in the 3′ untranslated regions of the majority of protein-encoding messenger ribonucleic acids (mRNAs) (3). Next to their pivotal role in almost any cellular process investigated to date, they are important regulators in a large and growing list of disease entities, including cancer, immunologic disease, and cardiovascular disease (4). A considerable number of miRNAs are now firmly established as crucial regulators of key aspects of myocardial and vascular disease (5). With the availability of synthetic miRNA inhibitors for in vivo application (6), disease-associated miRNAs were soon also manipulated in various cardiovascular disease models, some with remarkable effect sizes (7).

SEE PAGE 1801

The first miRNA-based therapy that was successfully tested in a cardiovascular disease model was directed against miR-21 (8). miR-21 is one of the strongest expressed miRNAs in various cardiac cell types, and it is preferentially expressed in non-myocyte cell types and further up-regulated in various cardiac diseases that are associated with cardiac fibrosis (8–11). Its inhibition in murine disease models was found to prevent the development of pressure overload-induced myocardial fibrosis and dysfunction but was also effective when given in established disease (8).

In follow-up studies, miR-21 was found to be strongly up-regulated in numerous non-cardiovascular diseases characterized by interstitial fibrosis of their parenchyma. As with myocardial fibrosis, inhibition of miR-21 had significant (and partially drastic) therapeutic effects in these disease models. For example, pharmacological inhibition or genetic deletion of miR-21 attenuated pulmonary fibrosis (12), kidney fibrosis (13), liver fibrosis (14), and skeletal muscle fibrosis (15).

A major obstacle, which to date has prevented the clinical development of multiple oligonucleotide-based therapies, is the relatively low extent to which these molecules enter cells upon systemic delivery (6). The liver and the kidney differ in this respect from most other organs, which has led to clinical studies aiming at miRNAs as targets. On the basis of proof-of-concept studies of miR-21 inhibition in animal models for Alport syndrome (a familial form of kidney fibrosis [13]), a phase I clinical trial has recently been completed (16), with a phase II trial currently enrolling (NCT02855268) (17). In comparison, delivery to the myocardium has been more challenging, yet a recent study reported efficient knockdown and therapeutic benefit for intracoronary application of antisense miR (antimiR)-92 directly (60 min) after myocardial ischemia in a pig model (18).

Here, we sought to test the applicability and therapeutic efficacy of local, intracoronary delivery of antimiR-21 in a clinically relevant large animal model of HF. To gain insight into the underlying effects on the transcriptional and cellular level, we devised a genetic deconvolution approach to characterize the effect of antimiR-21 on the pig cardiac transcriptome and the relative changes of myocardial cell types.

ABBREVIATIONS AND ACRONYMS

antimiR = antisense micro-ribonucleic acid

EF = ejection fraction

ERK = extracellular signal-regulated kinase

HF = heart failure

I/R = ischemia/reperfusion

LAD = left anterior descending coronary artery

LNA = locked nucleic acid

LV = left ventricular

MAP = mitogen-activated protein

miR, miRNA = micro-ribonucleic acid

mRNA = messenger ribonucleic acid

METHODS

PIG ISCHEMIA/REPERFUSION MODEL. German pigs (German landrace) were obtained from the Department of Veterinary Medicine at Ludwigs-Maximilians-Universität Munich (Oberschleißheim, Germany). Animal care and all experimental procedures were performed in accordance with German and National Institutes of Health animal legislation guidelines and were approved by the Bavarian Animal Care and Use Committee (AZ 55.2.-1-54-2532-26-09, 141-11, and 62-13). See the Supplemental Methods and Supplemental Tables 1 and 2 for details.

FLUOROSCOPY. Ejection fraction (EF) was determined using fluoroscopic image analysis. EF was acquired before ischemia and after 33 days of reperfusion.

HEMODYNAMIC MEASUREMENTS. Invasive monitoring of left ventricular (LV) function was obtained using a standard pressure tip catheter percutaneously introduced through the left carotid artery and aorta into the LV lumen (ADV500, Transonic, Ithaca, New York) under continuous monitoring of the

FIGURE 1 Efficiency of miR-21 Inhibition Using LNA-Modified Antisense miR-21

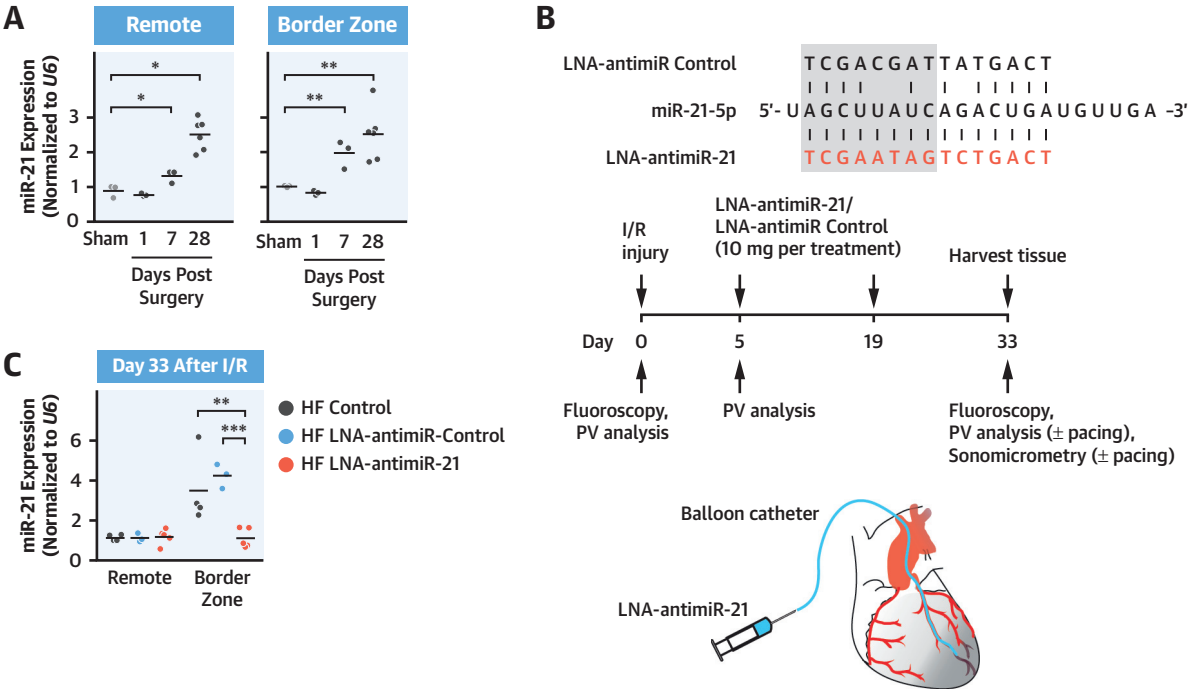

(A) Expression of miR-21 in post-ischemic myocardium. Sham, n = 3; ischemia/reperfusion (I/R) injury (n = 3 to 6). **(B)** Experimental strategy. Pigs underwent catheterization with balloon occlusion of the left anterior descending coronary artery (LAD) for 60 min, followed by reperfusion for 33 days. The micro-ribonucleic acid (miR) inhibitor locked nucleic acid (LNA)–modified antisense miR-21 (antimiR-21) was applied regionally with a catheter at day 5 and day 19 during reperfusion injury. Ten milligrams of LNA-antimiR-21 was infused into the LAD and the left circumflex coronary artery in a ratio of 3:2. **(Top)** Sequences of miR-21, LNA-antimiR-21, and LNA-antimiR-control. **Gray region** indicates the seed sequence, and bases complementary to miR-21 are shown in **red**. **(C)** Quantitative analysis of miR-21 expression after regional application of LNA-antimiR-21 or LNA-antimiR-control. Heart failure (HF) control, n = 4; HF LNA-antimiR-control, n = 3; HF LNA-antimiR-21, n = 5. Data are mean and individual values and were analyzed using 1-way analysis of variance (ANOVA) **(B)** or 2-way ANOVA **(C)** with the Sidak post-test. *p < 0.05, **p < 0.01 and ***p < 0.001. PV = pressure-volume.

pressure curves until the diastolic pressure indicated localization in the left ventricle (see Supplemental Methods).

AntimiR APPLICATION. The antimiRs were synthesized as fully phosphorothioated locked nucleic acid (LNA)/deoxyribonucleic acid mixmers (Exiqon, Vedbaek, Denmark). The antimiRs (10 mg each) were locally applied at days 5 and 19 (antegrade) into the left anterior descending coronary artery (LAD) using an over-the-wire balloon catheter.

QUANTIFICATION AND STATISTICAL ANALYSIS. Data are expressed as mean and individual values. Statistical analysis was performed using GraphPad Prism version 6 (GraphPad Software, La Jolla, California). Data distribution was assessed using the Shapiro-Wilk test for normality. Common variance was tested using the *F* test or Bartlett test for column datasets, and the Spearman rank correlation test of heteroscedasticity for grouped datasets. For datasets that did not pass the heteroscedasticity test, values were log-transformed prior to statistical testing. Differences among multiple means were assessed using either 1-way or 2-way analysis of variance followed by the Sidak test. The p values <0.05 were considered to indicate statistical significance.

For detailed methods, see the Supplemental Appendix.

RESULTS

INHIBITION OF miR-21 BY LOCAL DELIVERY OF LNA-antimiR-21. We first sought to determine the expression of miR-21 in LV myocardium of a large animal model of HF, namely, pigs subjected to transient occlusion (60 min) of the LAD. In a pilot experiment, animals were followed for 1, 7, or 28 days before euthanasia and removal of the hearts for further analysis (**Figure 1A**). Consistent with previous reports in mice (8), expression of miR-21 was

FIGURE 2 Inhibition of miR-21 Protects Pig Hearts From I/R-Induced Cardiac Hypertrophy and Myocardial Fibrosis

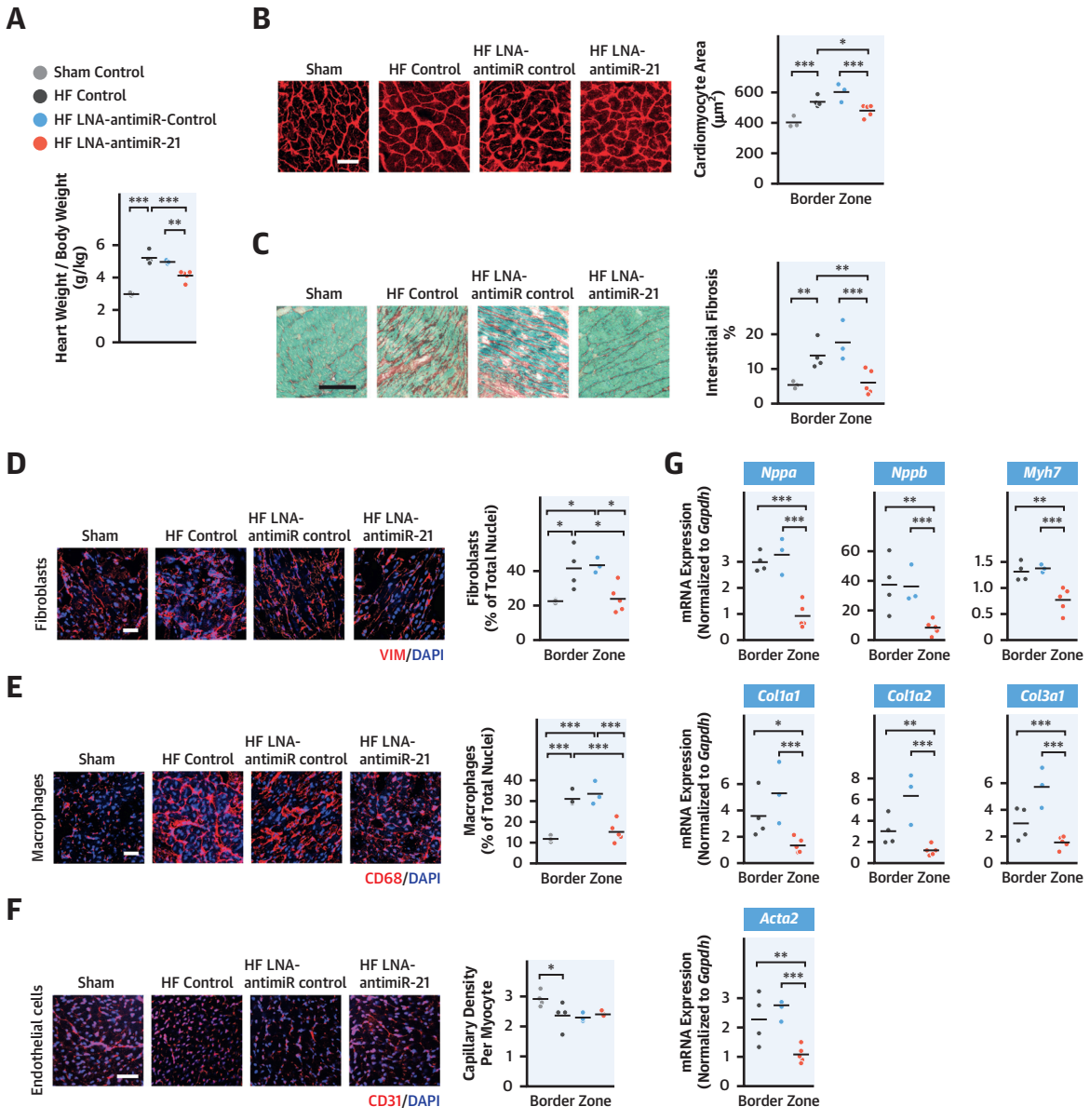

(A) Ratio of heart weight to body weight. **(B)** Wheat germ agglutinin staining in representative myocardial sections in the border zone of hearts **(left)**. Quantification of data **(right)**. **(C)** Representative staining of myocardial samples using Sirius red/Fast green **(left)**. Quantification of data **(right)**. **(D)** Quantitative analysis of vimentin staining (fibroblast marker) for the border zone of hearts. **(E)** Quantitative analysis of CD68 staining (macrophage marker) for the border zone of hearts. **(F)** Capillary density was determined by staining myocardial sections with an antibody against CD31 in the border region. Representative images and quantification. **(G)** Quantitative assessment of messenger ribonucleic acid (mRNA) levels of collagen genes (*Col1a1*, *Col1a2*, and *Col3a1*), smooth muscle actin (*Acta2*), and myocyte hypertrophy-associated genes (*Nppa*, *Nppb*, and *Myh7*). Scale bars: 50 µm **(B)**, 500 µm **(C,D)**. n > 300 cells with central nuclei per heart **(B)**. n > 10,000 cells per heart **(D–F)**. Sham control, n = 3; HF control, n = 4; HF LNA-antimiR control, n = 3; HF LNA-antimiR-21, n = 5. Data are mean and individual values and were analyzed using 1-way ANOVA with the Sidak post-test. *p < 0.05, **p < 0.01, and ***p < 0.001. Abbreviations as in Figure 1.

progressively up-regulated in both remote and border-zone regions of LV myocardium (Figure 1A). Because of these expression kinetics and a reported antiapoptotic role for miR-21 in cardiac myocytes in acute ischemia (19), we decided on the following experimental design: pigs were subjected to ischemia/reperfusion (I/R), left untreated for 5 days to allow scar formation, and then twice given (days 5

FIGURE 3 Catheter-Based Local Application of LNA-AntimiR-21 Improves Global and Regional Myocardial Function

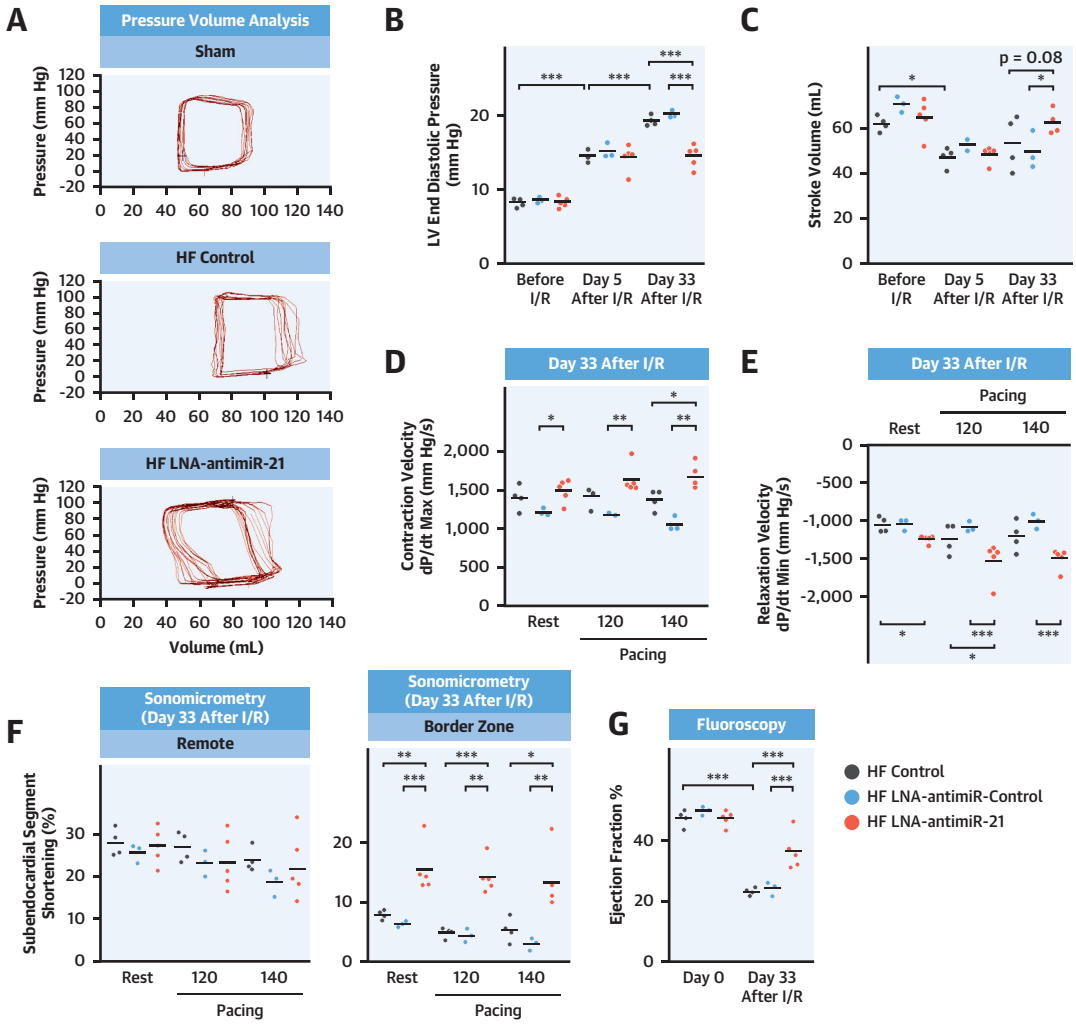

Pigs underwent percutaneous I/R injury (60 min for 33 days), and LNA-antimiR-21 or LNA-antimiR-control was applied regionally with a catheter at day 5 and day 19 during reperfusion injury. **(A)** Representative pressure-volume loop tracings obtained at day 33 after I/R. **(B to E)** Indexes of global myocardial function as measured by PV analysis. **(B)** Left ventricular (LV) end-diastolic pressure. **(C)** Stroke volume. **(D)** Contraction velocity. **(E)** Relaxation velocity of the left ventricle. **(F)** Subendocardial segment shortening as determined by sonomicrometry as a measure of regional myocardial function. Analysis was performed 33 days after I/R injury under rest or after pacing at 120 and 140 beats/min. **(G)** Ejection fraction as determined by fluoroscopy before I/R injury and at day 33 after reperfusion. HF control, n = 4; HF LNA-antimiR control, n = 3; HF LNA-antimiR-21, n = 5. Data are mean and individual values and were analyzed using 2-way ANOVA with the Sidak post-test. *p < 0.05, **p < 0.01, and ***p < 0.001. Abbreviations as in Figure 1.

and 19 after I/R) LNA-modified antimiR-21 (LNA-antimiR-21) locally into the coronary arteries (Figure 1B). We chose a phosphorothioate-modified, 15-nt, LNA/deoxyribonucleic acid mixmer design to inhibit miR-21 with high specificity and efficacy. Ten milligrams of LNA-antimiR-21 or control was infused into the LAD and the left circumflex coronary artery in a ratio of 3:2 and over a time period of 3 min/vessel, with concomitant occlusion of the vessel by an angioplasty balloon (Figure 1B). At 33 days after I/R injury, intracoronary delivery of LNA-antimiR-21 led to a significant reduction of miR-21 (−66%), as detected by quantitative reverse transcriptase polymerase chain reaction on RNA prepared from LV ischemic myocardium (Figure 1C). Interestingly, the repression of miR-21 appeared to preferentially occur

in the border zone compared with the remote region of the myocardium, suggesting preferential uptake in ischemic tissue. Regional application of LNA-antimiR-21 likewise did not alter miR-21 levels in other regions of the heart, right ventricle, left atria, and right atria (Supplemental Figure 1). Consistent with previous results of local antimiR application in pigs (18), we observed a modest but significant reduction of miR-21 in the kidney and in the lung (Supplemental Figure 1), organs known for very high uptake of systemic oligonucleotide therapeutics (20). Serum concentrations of routine clinical chemistry parameters for kidney and liver function were in the normal range, indicating intact kidney and liver function (Supplemental Table 3). Also, upon application of LNA-antimiR-21, we did not observe episodes of arrhythmia or deaths, which occurred only prior to the application of the antimiR (Supplemental Table 2). Taken together, catheter-based, local delivery of LNA-antimiR-21 was effective in long-term suppression of miR-21 in LV myocardium of a large animal model of HF.

INHIBITION OF miR-21 DECREASES I/R-INDUCED ADVERSE MYOCARDIAL REMODELING. We next determined the effect of LNA-antimiR-21 on myocardial remodeling (**Figure 2**). At 33 days after I/R, the 2 different treatment groups exhibited similar infarct sizes (Supplemental Figure 2A). Prominent adverse cardiac remodeling was observed at this time point, evident as a significant increase in the ratio of heart weight to body weight, cardiac myocyte hypertrophy, and cardiac fibrosis, all of which were significantly reduced in the LNA-antimiR-21-treated pigs (**Figures 2A to 2C**). We then assessed key pathological processes that have been associated with myocardial remodeling, namely, fibroblast proliferation, inflammation, and angiogenesis (**Figures 2D to 2F**). Immunofluorescent staining of LV myocardium indicated fibroblast proliferation and macrophage infiltration, both of which were significantly repressed by LNA-antimiR-21 compared with control-treated animals. In contrast, we found no evidence for alterations in capillary density in this model, nor was this affected by antimiR-21 (**Figure 2F**). Analysis of myocardial total RNA by quantitative reverse transcriptase polymerase chain reaction yielded a gene expression signature indicative of myocardial remodeling in other species, including humans, which was likewise significantly reversed in the LNA-antimiR-21 group (**Figure 2G**). Comparative analyses of remote LV myocardium indicated only minimal changes in the parameters characterizing myocardial remodeling (Supplemental Figures 2B to 2D).

CATHETER-BASED LOCAL DELIVERY OF LNA-antimiR-21 IMPROVES GLOBAL AND REGIONAL MYOCARDIAL FUNCTION. To evaluate the impact of miR-21 inhibition on cardiac function, invasive hemodynamic measurements (pressure-volume analysis) were carried out before ischemia (day 0) and at day 5 (before LNA-antimiR-21 administration) and 33 days post-ischemia (also with cardiac pacing to obtain rate-contraction relationships). This was complemented with contrast agent fluoroscopy before (day 0) and after (day 33) ischemia to determine EF and myocardial perfusion under resting conditions. Before animals were euthanized and tissue was harvested on day 33, sonomicrometry with cardiac pacing was performed upon implantation of ultrasonic crystals into the border zone (10 mm distal to the occlusion site) and remote myocardium (see scheme in **Figure 1B** for an overview of the experimental strategy).

The control-treated animals displayed a marked decline in global myocardial function, with increased LV end-diastolic pressure, decreased LV stroke volume, and a negative rate-contraction relationship indicative of overt HF (**Figures 3A to 3E**). In contrast, treatment with LNA-antimiR-21 significantly prevented a decline in cardiac function (**Figures 3A to 3E**). Consistently, LNA-antimiR-21 application led to a significant gain of functional reserve of the left ventricle, as evidenced by a positive rate-contraction relationship (**Figures 3D and 3E**). Analysis of LV volumes likewise indicated a significant reduction of LV end-systolic volume (HF, 58.5 ± 3.4 ml; HF LNA-antimiR-control, 58 ± 0.4 ml; and HF LNA-antimiR-21, 40.2 ± 5.3 ml), while the modest reduction in LV end-diastolic volume observed with LNA-antimiR-21 did not reach statistical significance (HF, 112.7 ± 3.5 ml; HF LNA-antimiR-control, 107.6 ± 3 ml; and HF LNA-antimiR-21, 103 ± 2.7 ml). As an independent measure of LV function, we used sonomicrometry to determine subendocardial segment shortening (**Figure 3F**). In line with the hemodynamic analyses, LNA-antimiR-21 improved regional contractility compared with LNA-antimiR-control-treated animals under both resting and pacing (140 beats/min) conditions (**Figure 3F**). Fluoroscopy upon injection of a contrast agent likewise indicated a marked decline in EF at day 33, which was prevented in the LNA-antimiR-21 group (**Figure 3G**). Although our study design did not aim for a quantitative determination of tissue perfusion such as by magnetic resonance imaging or positron emission tomography, we did not observe any difference between the groups with regard to coronary flow (by contrast agent injection) with a TIMI

FIGURE 4 Differential Expression Analysis Reveals Derepression of miR-21 Targets After LNA-AntimiR-21 Application

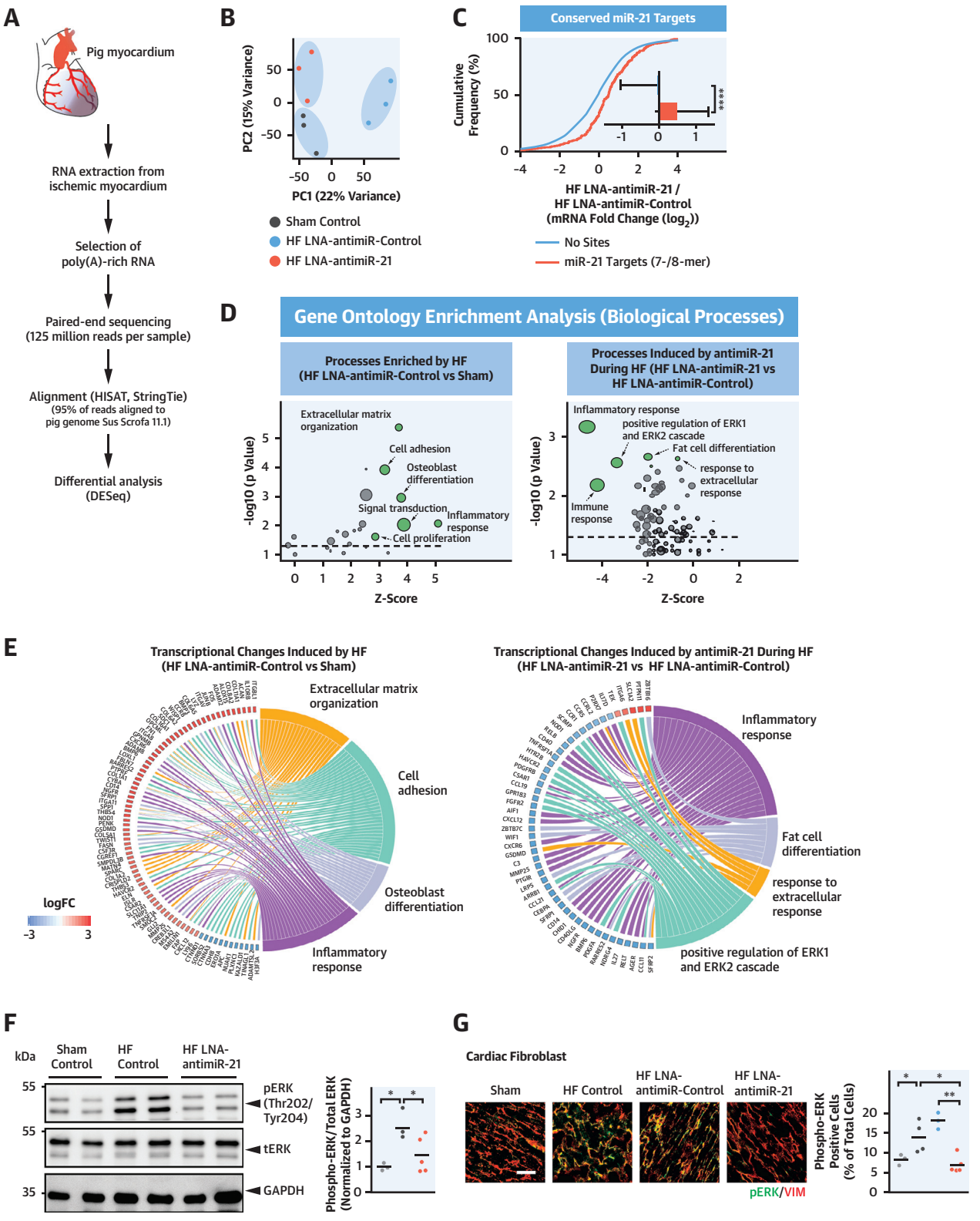

Continued on the next page

(Thrombolysis In Myocardial Infarction) flow grade of 3, indicating normal perfusion of the LAD, including its microcirculation (data not shown). Finally, the effect of LNA-antimiR-21 appeared to be dose dependent, as our data obtained from treatment with 4 instead of 10 mg of oligonucleotide suggest (Supplemental Figure 3). In summary, these findings demonstrate that local application of a miR-21 inhibitor significantly improved cardiac function in this model of post-ischemic HF.

AntimiR-21 NORMALIZES TRANSCRIPTOMIC SIGNATURES OF FAILING PIG MYOCARDIUM. We finally sought to directly determine the consequences that interfering with miR-21 has on the disease-associated gene expression signature in this large animal model. Using TruSeq Illumina sequencing of polyA-enriched RNA isolated from LV ischemic myocardium (border zone) treated with LNA-antimiR-21 or control and from sham-treated animals ($n = 3$ from each group) yielded approximately 126.6 million reads per sample after removing the adaptors and filtering (>99.9% of reads qualified). Mapping the reads to the pig genome (*Sus scrofa* version 11.1), we were able to successfully align 112 million reads (**Figure 4A**, Supplemental Figure 4). This corresponds to 95 ± 0.4% of all reads aligned with high confidence, illustrating the high quality of the dataset, which to our knowledge is the first extensive deep sequencing dataset of myocardial disease in the adult pig.

A principal-component analysis revealed clear separation among and high homogeneity within the 3 different experimental groups studied, underlining the validity of this dataset for subsequent analyses (**Figure 4B**). Ischemia led to a pronounced deregulation of the pig cardiac transcriptome, which was partially reverted by antimiR-21 treatment.

To assess whether these transcriptome changes indeed related to the modulation of miR-21 activity in the myocardium, we determined the distributions of mRNA fold changes for all genes and compared them with those of conserved miR-21 targets, predicted by TargetScan Human 7 (**Figure 4C**). Inhibition of miR-21 resulted in significant derepression of miR-21 targets compared with mRNAs containing no sites for miR-21 (**Figure 4C**).

AntimiR-21 INHIBITS PRO-FIBROTIC AND INFLAMMATORY TRANSCRIPTIONAL SIGNATURES IN FAILING MYOCARDIUM. We then sought to identify the biological processes primarily activated during HF and modulated by interfering with miR-21. Gene Ontology enrichment analysis of all mRNAs deregulated in HF (log fold change >2 or log fold change <−2 and $q < 0.05$) showed enrichment for processes related to tissue remodeling, including extracellular matrix organization, cell adhesion, osteoblast differentiation, and inflammatory response (**Figures 4D and 4E**, left). Interfering with miR-21 had the strongest effect on the inflammatory and immune response, followed by repression of extracellular signal-regulated kinase (ERK)-mitogen-activated protein (MAP) kinase (**Figures 4D and 4E**, right). To further validate the latter and to determine whether this transcriptional signature resulted in altered protein activity of ERK-MAP kinase, we performed western blotting and immunofluorescence staining for activated MAP kinase 3 (phosphorylated ERK) on cardiac tissue (**Figures 4F and 4G**). AntimiR-21 resulted in a significant inhibition of HF-induced ERK-MAP kinase activity (**Figure 4F**). Remodeling-associated ERK activation and its repression by antimiR-21 were found to primarily occur in cardiac fibroblasts (**Figure 4G**).

FIGURE 4 Continued

(A) Scheme for ribonucleic acid (RNA) sequencing. RNA sequencing libraries were generated from 4 μg total RNA samples isolated from myocardial ischemic tissue using TruSeq Stranded mRNA sample preparation kit. Sequencing was carried out on a HiSeq4000 (Illumina), and the analysis was carried out using an in-house Galaxy platform. $n = 3$ per group. **(B)** Principal-component analysis. Principal component 1 (PC1; x-axis) represents 59.5%, and principal component 2 (PC2; y-axis) represents 40.5% of total variation in the data (transcripts per million [TPM] ≥3; $n = 8{,}432$). **(C)** Cumulative distribution and median fold change plots of differential expression for all genes and broadly conserved miR-21 targets containing 8-mer, 7-mer-m8, or 7-mer-A1 binding sites as predicted by TargetScan Human version 7. Bar graphs show median mRNA fold change with interquartile range. Data were analyzed using the Kolmogorov-Smirnov test. ****$p < 0.0001$. **(D)** Gene Ontology (GO) enrichment of biological processes for highly deregulated genes (log fold change [logFC] >2 or <−2, adjusted p value < 0.05) between HF LNA-antimiR-control and sham **(left)** and between HF LNA-antimiR-21 and HF LNA-antimiR-control **(right)**. **Gray dotted line** indicates $p < 0.05$ for the GO terms. **(E)** Chord diagram showing the deregulated genes and their associated GO terms. **(F)** Immunoblot directed against phosphorylated extracellular signal-regulated kinase (pERK) and unphosphorylated ERK (tERK) performed on myocardial tissue lysates. GAPDH was used as loading control. **(G)** Percentage of pERK-positive cardiac fibroblasts in the pig myocardial tissue. Immunofluorescent staining was performed on myocardial sections against pERK, vimentin (VIM; a mesenchymal cell marker), and CD31 (an endothelial cell marker). Nuclei was stained with DAPI. Cells that were positive for VIM and negative for CD31 were considered cardiac fibroblasts. Scale bar: 50 μm. Sham control, $n = 3$; HF control, $n = 4$; HF LNA-antimiR-control, $n = 3$; HF LNA-antimiR-21, $n = 5$. Data denote mean and individual values and were analyzed using 1-way ANOVA. *$p < 0.05$ and **$p < 0.01$. Abbreviations as in **Figure 1**.

FIGURE 5 Next-Generation RNA Sequencing Coupled With Genetic Deconvolution Reveals a Critical Role of Macrophages and Fibroblasts in AntimiR-21-Treated Pig Myocardium

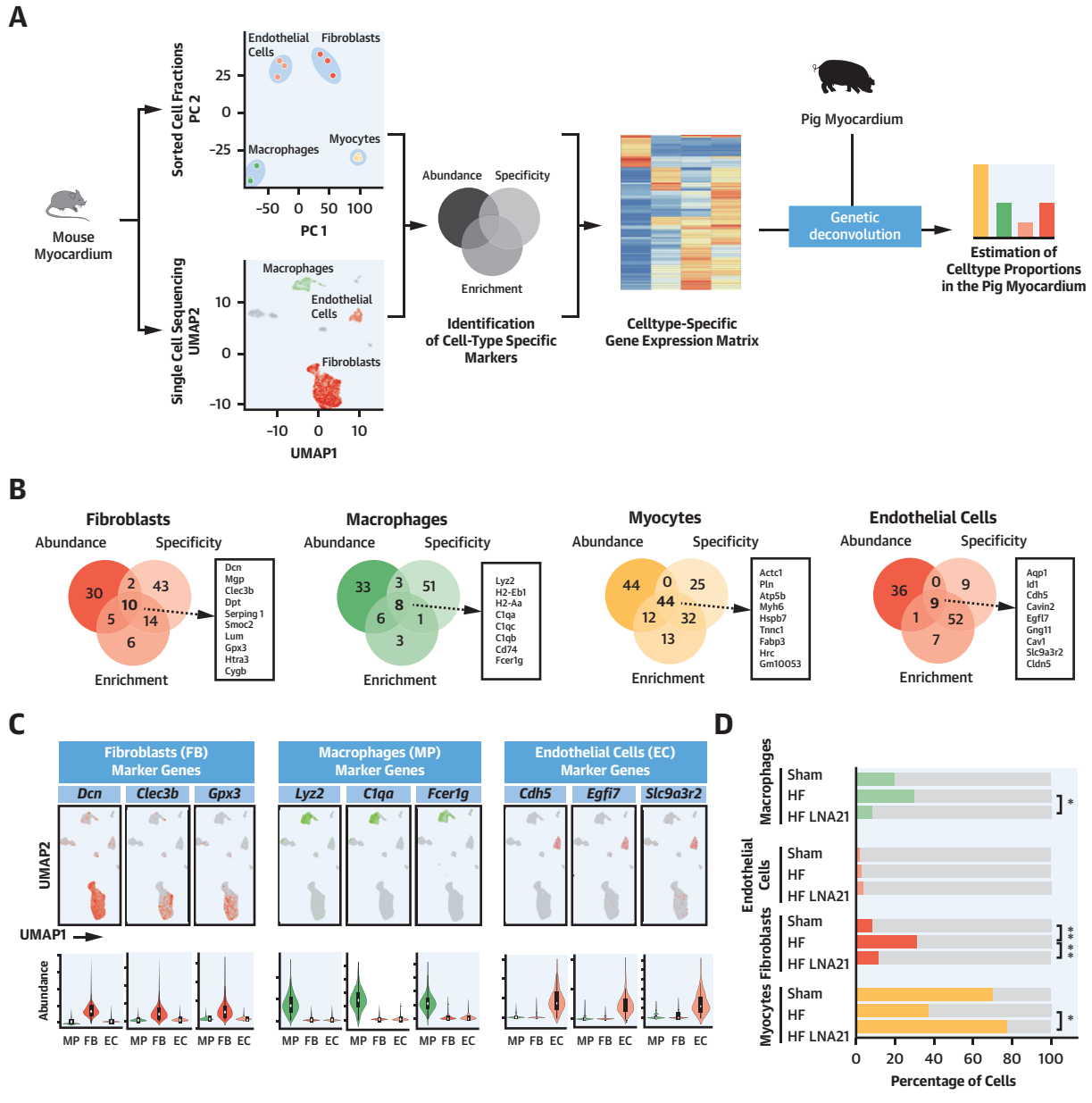

(A) Overview of genetic deconvolution. **(B)** Intersections among genes for consensus rankings on the basis of abundance, specificity, and enrichment for the gene across cell types. **(C)** UMAP feature and violin plots of the top 3 enriched genes in the signature matrix for macrophages, endothelial cells, and fibroblasts. **(D)** Relative cell type proportion estimates for pig myocardium from bulk and single-cell RNA expression for myocytes, endothelial cells, fibroblasts, and macrophages. Sham control, n = 3; HF control, n = 3; HF LNA-antimiR-21, n = 5. Data are mean and individual values and were analyzed using 1-way ANOVA with the Sidak post-test. *p < 0.05 and **p < 0.01. Abbreviations as in Figure 1 and 4.

A GENETIC DECONVOLUTION APPROACH FOR THE PIG IDENTIFIES CARDIAC MACROPHAGES AND FIBROBLASTS AS THE KEY CELL TYPES AFFECTED BY antimiR-21 TREATMENT. The transcriptional changes observed in the myocardium putatively originate from changes in cell states but also from variations in cell type proportions. To analyze the latter, we sought to develop a genetic deconvolution approach for the pig. This requires the generation of a signature matrix that represents cell type-specific

CENTRAL ILLUSTRATION **AntimiR-21 Prevents Myocardial Remodeling Through Its Effects on Cardiac Macrophages and Fibroblasts**

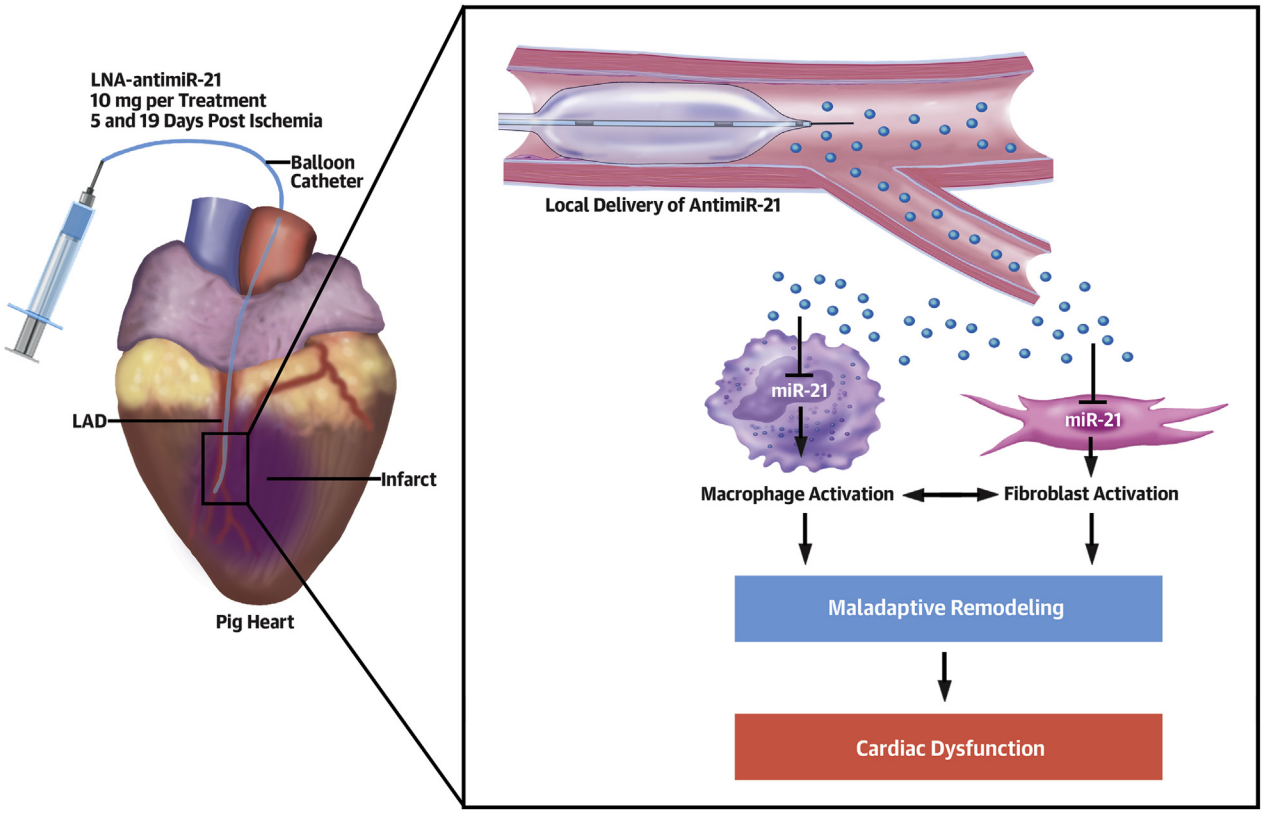

Hinkel, R. et al. J Am Coll Cardiol. 2020;75(15):1788–800.

MiR-21 is a central regulator of cardiac fibrosis, and its inhibition in small-animal models has been shown to be an effective antifibrotic strategy in various organs, including the heart. Here, we provide evidence that intracoronary infusion of antimiR-21 is feasible and therapeutically effective in a pig model of post-ischemic cardiac remodeling and heart failure. Catheter-based regional application of locked nucleic acid (LNA)–antimiR-21 might offer a novel therapeutic option to prevent the development of heart failure after myocardial infarction. Abbreviations as in Figure 1.

gene expression and that forms the basis to deconvolve a bulk RNA-seq dataset. We encountered a number of obstacles that precluded us from relying solely on single-cell datasets from small animal species to generate this signature matrix: 1) most datasets that comprise all major cardiac cell types (typically from droplet-based platforms) contain small numbers of myocytes, thereby precluding proper assignment to this cell type; 2) populations that are characterized only by genes of low abundance; and 3) cell types that make up only a small proportion of all cells. To overcome these limitations, we therefore included deep transcriptome data derived from the 4 principal myocardial cell types (myocytes, fibroblasts, macrophages, and endothelial cells) sorted from mouse heart and used them in addition to a mouse single-cell RNA-seq dataset (reprocessed data reported by Skelly et al. [21]) (Figure 5A). We then identified the top enriched, highly specific, and most abundant genes in each cell type of interest and combined these for the single-cell RNA-seq and deep RNA-seq datasets (Figures 5A and 5B). Finally, we computed the overlap regarding the top abundant, specific, and enriched mRNAs for all 4 cell types (Figure 5B), and these markers were then used to build the signature matrix for deconvolution. Figure 5C illustrates the high cell type specificity of thereby identified exemplary markers (and thereby the validity of our signature matrix) in feature plots of their expression in cardiac single-cell RNA-seq data (top) and by quantitative analysis of their expression (bottom). We then applied this novel genetic deconvolution approach to determine the relative cell type proportions under

sham conditions, upon cardiac remodeling during HF, and the effect of antimiR-21 (**Figure 5D**). Failing myocardium was characterized by prominent increases in macrophage and fibroblast numbers, an effect that was largely reversed by treatment with antimiR-21. Taken together, this unbiased approach to analyze RNA-seq data from cardiac tissue is able to determine cell fractions in a quantitative manner and independently corroborates that treatment with antimiR-21 led to a restitution of the relative cell fractions resembling homeostatic conditions (**Figure 5D**).

DISCUSSION

This study demonstrated the applicability and therapeutic efficacy of local delivery of antimiR-21 in a pig model of HF (**Central Illustration**). In recent years, a number of miRNAs have been demonstrated to regulate myocardial remodeling (5), and synthetic inhibitors against some of them have shown therapeutic effects in preventing myocardial disease (7,8,22). All of these studies have in common that comparably high doses of oligonucleotides were used, ranging from 2 to 80 mg/kg body weight. These doses cannot be easily scaled to humans, both for economic reasons and because of side effects that can be expected with such high substance loads (7,23). Targeting miRNA inhibitors to the desired site of action has been proposed as a solution to this dilemma but so far has been implemented only for a few organs (24). Most advanced is the targeting of oligonucleotides to the liver, where the covalent coupling to trivalent *N*-acetylgalactosamine clusters facilitates cellular uptake of therapeutic oligonucleotides through a hepatocyte-specific transporter system (6). With regard to the myocardium, such an approach is entirely lacking at present. Also, in the case of miR-21, this would be particularly challenging, as we have previously shown miR-21 to exert its detrimental functions primarily in nonmyocyte cell types that are present throughout the body (11). An alternative approach to target a specific organ is to localize its application. Cardiac catheterization has become a routine procedure in clinical cardiology, with the vast majority of all patients presenting with an acute coronary syndrome undergoing this intervention (25). Complications of cardiac catheterization have become a very rare event, allowing a low threshold for its application. Here, we applied antimiR-21 through the related coronary arteries, which offers the advantage of preferential exposure of the injured tissue to high concentrations of the antimiR. Interestingly, our data indicate that after ischemia, uptake of antimiR-21 in the myocardium appears facilitated, potentially because of leakiness of endothelia and dissolution of the extracellular matrix (**Figure 1C**, Supplemental Figure 1), supporting the idea of further concentrating antimiR-21 at the site of injury.

For the present study, we specifically sought to mimic a clinical scenario in which myocardial remodeling is common and miR-21 would exert an important pathophysiological role. Therefore, we chose a model of 1-h occlusion of the LAD and reperfusion, which led to a large infarct area of about 30% of the left ventricle (Supplemental Figure 2) and induction of HF. Despite established rapid interventional reperfusion strategies, this outcome may also occur in a distinct cohort of patients with ST-segment elevation myocardial infarction, for example, after prolonged ischemia intervals or after the low- or no-reflow phenomenon (see, e.g., Niccoli et al. [26]), which are clearly associated with worse outcomes over time. In our model of I/R-induced HF, profound deregulation of the transcriptome occurred, including up-regulation of miR-21, a finding that was originally reported in pressure-overloaded myocardium and in human myocardium from patients with dilated cardiomyopathy (8). In the years following its original description, up-regulation of miR-21 has been reported as a hallmark of myocardial remodeling originating from causes as diverse as pressure overload, myocardial infarction, and atrial fibrillation. Subsequently, multiple studies have demonstrated the therapeutic efficacy of inhibiting miR-21 in the respective disease models (8,9,27). Yet overexpressing miR-21 in myocytes protected from myocyte apoptosis during acute ischemia (19). In line with such a suspected beneficial role of miR-21 in cardiac myocytes, we and others recently reported modest or neutral effects for global genetic deletion of miR-21 (11,28), whereas deletion in myocytes was detrimental and that in nonmyocytes provided cardioprotection (11). Together with the finding that cardiac miR-21 was not up-regulated acutely but rather progressively and several days after myocardial ischemia, these arguments made us decide to undertake the first application of antimiR-21 after the initial phase of cell death, that is, on day 5, with a second application on day 19 to extend the duration of suppression of pathological miRNA activity.

In this model, inhibition of miR-21 lead to sustained reshaping of the myocardial transcriptome 4 weeks after initiation of the treatment, suggesting a remarkably long-lasting suppression of miR-21 activity, a notion that is in line with previous observations for LNA-based treatment regimens (24). The respective RNA sequencing-based transcriptome datasets

accompanying this study are, to our knowledge, the first obtained in diseased pig myocardium.

We did not aim to delineate the precise molecular mechanisms (direct targets probably range in the tens to hundreds) through which miR-21 exerts its effects. Instead, we continue to pursue this task in defined cellular models and in model organisms such as mice that allow cell type–specific and timed genetic manipulations. Along with obtaining evidence for the relevance of miR-21 in regulating the cardiac transcriptome, such an analysis of an entire tissue transcriptome can likewise provide cues on the biological processes primarily affected. It was such unbiased Gene Ontology analysis that identified inflammation-related and MAP kinase signaling to be most significantly affected by manipulation of miR-21. Not only is this finding in good agreement with a considerable number of previous studies on miR-21 conducted in different models, but we could also validate the targetome data with independent methodology, supporting the role of miR-21 in controlling myocardial MAP kinase activity (**Figures 4F and 4G**).

Knowledge of cell type composition in the diseased myocardium after antimiR-21 treatment is an essential step toward understanding as to where and how antimiR-21 exerted its therapeutic effects. This study is the first to use a genetic deconvolution approach to determine the abundance of the major myocardial cell types of the pig heart. Our deconvolution algorithm enabled us to reach a high degree of confidence with regard to cell type assignment despite relatively small numbers of marker genes. Instrumental to this were recent refinements of algorithms developed for the mouse, such as the integration of cell type specificity and enrichment coupled to single cell RNA-seq data from the mouse. Together (see also scheme in **Figure 5A**), this approach allowed us to develop the first signature matrix for genetic deconvolution of the pig heart. This matrix can be downloaded from the publisher's web site and should be applicable to a wide variety of future studies that involve transcriptome analyses of the pig heart. Furthermore, our deconvolution methodology may be further refined upon the availability of additional datasets (e.g., single-cell RNA-seq datasets, datasets from additional cell types), and it should also be applicable to generate signature matrices for other organs and species.

Our analysis indicates that antimiR-21 led to reduction in macrophage infiltration as well as fibroblast proliferation. To avoid potential detrimental consequences of promoting cardiomyocyte death by antimiR-21 in the acute ischemic setting (19), we deliberately designed this study to not interfere with this protective function of miR-21 in acute ischemia but with its presumed detrimental role in promoting myocardial remodeling in the post-ischemic phase. Indeed, antimiR-21 did not promote the loss of myocytes (the relative reduction seen in the genetic deconvolution analysis is a necessary consequence from the inherent normalization of the combined cell numbers to 100%). Our complementary data on the absolute determination of fibroblasts and endothelial cell numbers by immunofluorescence (see **Figures 2D and 2F**), although certainly not as unbiased and quantitative as the genetic deconvolution approach, support this interpretation. At the same time, antimiR-21 may prevent (also indirectly through its effects other cell types) a further, low-level loss of ventricular myocytes that accompanies post-ischemic myocardial remodeling (19). Although this study was not designed to assess the extent and mechanism of myocyte loss early after ischemic injury, TUNEL staining for apoptosis of myocyte and mesenchymal cells indicated a reduction of apoptosis (0.04 ± 0.01 vs. 0.02 ± 0.01 in HF control vs. HF LNA-anti-miR-21; $p < 0.05$), with approximately one-half of the TUNEL-positive cells staining positive for troponin T as a myocyte marker (data not shown).

STUDY LIMITATIONS. Although our strategy of applying antimiR-21 locally achieved lasting and therapeutically effective knockdown of miR-21 in the myocardium post-ischemia, there was still considerable knockdown of miR-21 in the lung and kidney. This was not unexpected and has been reported for other cardiac oligonucleotide-based therapies (20). However, extracardiac delivery of a potent therapeutic molecule may cause unwanted side effects in these organs. Future therapeutic modalities such as (e.g., nanoparticle-based) carrier systems, antibody conjugates, and cell type–specific targeting moieties (7) will likely help overcome these current limitations. Also, the infarct size is relatively large and the follow-up in our study is relatively short with respect to the average situation in humans. We used a model of large infarct size, as patients with large infarctions pose an unmet clinical need for specific adjunctive therapy during reperfusion. Our results suggest that interference with myocardial remodeling will eventually prove its effectiveness with regard to hard endpoints, in appropriate study designs with prolonged follow-up of patients with infarcts.

CONCLUSIONS

Taken together, our study provides the first evidence of the feasibility and therapeutic efficacy of antimiR-21 in a large animal model of myocardial ischemia and

suggests the further development of this therapeutic modality.

ACKNOWLEDGMENTS The authors thank Sabine Brummer for cardiac histology and Elisabeth Raatz and Cuong Kieu for expert technical assistance.

ADDRESS FOR CORRESPONDENCE: Dr. Stefan Engelhardt, Institut für Pharmakologie und Toxikologie, Technische Universität München, Biedersteiner Strasse 29, 80802 München, Germany. E-mail: stefan.engelhardt@tum.de. OR Dr. Christian Kupatt, Technische Universität München, 1. Medizinische Klinik, Klinikum rechts der Isar, Ismaninger Strasse 22, 81675 München, Germany. E-mail: christian.kupatt@tum.de.

PERSPECTIVES

COMPETENCY IN MEDICAL KNOWLEDGE: Patients with myocardial infarction develop myocyte hypertrophy and fibrosis through dysregulation of specific miRNAs, often leading to HF and mortality. Intracoronary administration of antimiR-21 in a pig model of myocardial infarction prevents adverse remodeling resulting from myocardial fibrosis and improves cardiac function.

TRANSLATIONAL OUTLOOK: Clinical studies are needed to assess the safety and efficacy of catheter-based intracoronary administration of LNA-antimiR-21 in patients with acute myocardial infarction.

REFERENCES

1. Bahit MC, Kochar A, Granger CB. Post-myocardial infarction heart failure. J Am Coll Cardiol HF 2018;6:179–86.

2. Pellicori P, Khan MJI, Graham FJ, Cleland JGF. New perspectives and future directions in the treatment of heart failure. Heart Fail Rev 2020;25:147–59.

3. Bartel DP. Metazoan microRNAs. Cell 2018;173:20–51.

4. Mendell JT, Olson EN. MicroRNAs in stress signaling and human disease. Cell 2012;148:1172–87.

5. Thum T, Condorelli G. Long noncoding RNAs and microRNAs in cardiovascular pathophysiology. Circ Res 2015;116:751–62.

6. Khvorova A, Watts JK. The chemical evolution of oligonucleotide therapies of clinical utility. Nat Biotechnol 2017;35:238–48.

7. Lu D, Thum T. RNA-based diagnostic and therapeutic strategies for cardiovascular disease. Nat Rev Cardiol 2019;16:661–74.

8. Thum T, Gross C, Fiedler J, et al. MicroRNA-21 contributes to myocardial disease by stimulating MAP kinase signalling in fibroblasts. Nature 2008;456:980–4.

9. Cardin S, Guasch E, Luo X, et al. Role for microRNA-21 in atrial profibrillatory fibrotic remodeling associated with experimental postinfarction heart failure. Circ Arrhythmia Electrophysiol 2012;5:1027–35.

10. Lorenzen JM, Schauerte C, Hubner A, et al. Osteopontin is indispensible for AP1-mediated angiotensin II-related miR-21 transcription during cardiac fibrosis. Eur Heart J 2015;36:2184–96.

11. Ramanujam D, Sassi Y, Laggerbauer B, Engelhardt S. Viral vector-based targeting of miR-21 in cardiac non-myocyte cells reduces pathologic remodeling of the heart. Mol Ther 2016;24:1939–48.

12. Liu G, Friggeri A, Yang Y, et al. miR-21 mediates fibrogenic activation of pulmonary fibroblasts and lung fibrosis. J. Exp Med 2010;207:1589–97.

13. Chau BN, Xin C, Hartner J, et al. MicroRNA-21 promotes fibrosis of the kidney by silencing metabolic pathways. Sci Transl Med 2012;4:121ra18.

14. Zhang J, Jiao J, Cermelli S, et al. miR-21 inhibition reduces liver fibrosis and prevents tumor development by inducing apoptosis of $CD24^{+}$ progenitor cells. Cancer Res 2015;75:1859–67.

15. Ardite E, Perdiguero E, Vidal B, Gutarra S, Serrano AL, Muñoz-Cánoves P. PAI-1-regulated miR-21 defines a novel age-associated fibrogenic pathway in muscular dystrophy. J Cell Biol 2012;196:163–75.

16. A study of RG-012 in subjects with Alport syndrome. Available at: https://clinicaltrials.gov/ct2/show/NCT03373786. Accessed March 4, 2020.

17. Study of weekly RG-012 injections in patients with Alport syndrome. Available at: https://clinicaltrials.gov/ct2/show/NCT02855268. Accessed March 4, 2020.

18. Hinkel R, Penzkofer D, Zühlke S, et al. Inhibition of microRNA-92a protects against ischemia/reperfusion injury in a large-animal model. Circulation 2013;128:1066–75.

19. Sayed D, He M, Hong C, et al. MicroRNA-21 is a downstream effector of AKT that mediates its antiapoptotic effects via suppression of Fas ligand. J Biol Chem 2010;285:20281–90.

20. Stenvang J, Petri A, Lindow M, Obad S, Kauppinen S. Inhibition of microRNA function by antimiR oligonucleotides. Silence 2012;3:1.

21. Skelly DA, Squiers GT, McLellan MA, et al. Single-cell transcriptional profiling reveals cellular diversity and intercommunication in the mouse heart. Cell Rep 2018;22:600–10.

22. Sassi Y, Avramopoulos P, Ramanujam D, et al. Cardiac myocyte miR-29 promotes pathological remodeling of the heart by activating Wnt signaling. Nat Commun 2017;8:1614.

23. Li Z, Rana TM. Therapeutic targeting of microRNAs: current status and future challenges. Nat Rev Drug Discov 2014;13:622–38.

24. Juliano RL. The delivery of therapeutic oligonucleotides. Nucleic Acids Res 2016;44:6518–48.

25. Bashore TM, Balter S, Barac A, et al. 2012 American College of Cardiology Foundation/Society for Cardiovascular Angiography and Interventions expert consensus document on cardiac catheterization laboratory standards update: A report of the American College of Cardiology Foundation Task Force. J Am Coll Cardiol 2012;59:2221–305.

26. Niccoli G, Burzotta F, Galiuto L, Crea F. Myocardial No-reflow in humans. J Am Coll Cardiol 2009;54:281–92.

27. Adam O, Löhfelm B, Thum T, et al. Role of miR-21 in the pathogenesis of atrial fibrosis. Basic Res Cardiol 2012;107:278.

28. Patrick DM, Montgomery RL, Qi X, et al. Stress-dependent cardiac remodeling occurs in the absence of microRNA-21 in mice. J Clin Invest 2010;120:3912–6.

KEY WORDS cardiac disease, fibrosis, microRNA, miR-21, porcine model of heart failure

APPENDIX For supplemental methods, references, tables, and figures, please see the online version of this paper.